⌘ *Author's Choice*

THE JOURNAL OF BIOLOGICAL CHEMISTRY VOL. 287, NO. 11, pp. 8561–8570, March 9, 2012

The Role of the N-Domain in the ATPase Activity of the Mammalian AAA ATPase p97/VCP*[S]

Received for publication, September 9, 2011, and in revised form, January 18, 2012 Published, JBC Papers in Press, January 23, 2012, DOI 10.1074/jbc.M111.302778

Hajime Niwa[1], **Caroline A. Ewens, Chun Tsang, Heidi O. Yeung, Xiaodong Zhang, and Paul S. Freemont**[2]

From the Centre for Structural Biology, Division of Molecular Biosciences, Faculty of Natural Sciences, Imperial College London, London SW7 2AZ, United Kingdom

Background: p97/VCP disease-linked mutations increase ATPase activity and destabilize the N-D1 domain interaction.
Results: Increased N-domain flexibility in p97/VCP increases ATPase activity, whereas locking down the N-domain decreases it.
Conclusion: The p97/VCP N-domain position relative to the D1 ring is linked to ATP hydrolysis ability.
Significance: p97/VCP N-domain conformational changes cause transitions between an active and inactive state.

p97/valosin-containing protein (VCP) is a type II ATPase associated with various cellular activities that forms a homohexamer with each protomer containing an N-terminal domain (N-domain); two ATPase domains, D1 and D2; and a disordered C-terminal region. Little is known about the role of the N-domain or the C-terminal region in the p97 ATPase cycle. In the p97-associated human disease inclusion body myopathy associated with Paget disease of bone and frontotemporal dementia, the majority of missense mutations are located at the N-domain D1 interface. Structure-based predictions suggest that such mutations affect the interaction of the N-domain with D1. Here we have tested ten major inclusion body myopathy associated with Paget disease of bone and frontotemporal dementia-linked mutants for ATPase activity and found that all have increased activity over the wild type, with one mutant, $p97^{A232E}$, having three times higher activity. Further mutagenesis of $p97^{A232E}$ shows that the increase in ATPase activity is mediated through D2 and requires both the N-domain and a flexible ND1 linker. A disulfide mutation that locks the N-domain to D1 in a coplanar position reversibly abrogates ATPase activity. A cryo-EM reconstruction of $p97^{A232E}$ suggests that the N-domains are flexible. Removal of the C-terminal region also reduces ATPase activity. Taken together, our data suggest that the conformation of the N-domain in relation to the D1-D2 hexamer is directly linked to ATP hydrolysis and that the C-terminal region is required for hexamer stability. This leads us to propose a model where the N-domain adopts either of two conformations: a flexible conformation compatible with ATP hydrolysis or a coplanar conformation that is inactive.

Mammalian p97, a protein that is highly abundant in cells, interacts with a diverse group of adaptor proteins to perform a variety of essential cellular processes, such as endoplasmic reticulum-associated degradation (1–3), transcription factor processing (4), nuclear envelope reconstruction (5), membrane fusion (6), postmitotic Golgi reassembly (7), spindle disassembly (8), and cell cycle control (9). These activities are at least in part associated with the ubiquitin-proteasome system, in which p97 binds poly-ubiquitylated proteins and several other ubiquitin-interacting proteins to participate in the delivery of ubiquitylated substrates to the 26 S proteasome for degradation. In the endoplasmic reticulum-associated degradation pathway, which is one of the most extensively studied among p97 cellular functions, p97 plays a key role in cooperating with adaptor proteins to translocate and chaperone misfolded proteins from the endoplasmic reticulum membrane to the proteasome (10, 11) in an ATP-dependent fashion, although the exact role of the ATPase activity of p97 is not entirely clear (12, 13).

p97 is a type II ATPase associated with various cellular activities) ATPase (AAA)[3] characterized by the presence of two highly conserved ATPase domains, each featuring Walker A and B motifs (14). Crystal structures of p97 show a homo-hexamer with two ring layers that encompass the D1 (amino acids 209–463 in murine p97) and D2 domains (amino acids 482–764) (15, 16). Although both D1 and D2 domains comprise the necessary motifs for ATP binding and hydrolysis, the D1 domain has less ATPase activity than D2. Its primary responsibility appears to be p97 hexamerization (17, 18). In contrast, the D2 domain confers most of the ATPase activity and is considered to be conformationally dynamic through the ATPase cycle (19, 20). p97 contains a third domain, the N-terminal domain (or N-domain, amino acids 1–192), which is connected to D1 by a flexible linker and is positioned coplanar with the D1 ring in crystal structures. The C-terminal region of p97 is not observed in the crystal structures. It is known to bind a subset of cofactors and can be phosphorylated, but its structure and significance are unknown.

The main function of the N-domain is to mediate the binding of cofactors and ubiquitylated protein substrates. Although only two conformations have been observed in p97 crystals (16,

* This work was supported by the Wellcome Trust.
⌘ *Author's Choice*—Final version full access.
[S] This article contains supplemental data, Table S1, and Figs. S1–S4.
[1] Present address: Department of Biology, Faculty of Sciences, Kyushu University Graduate School, Higashi-ku, Fukuoka, 812-8581, Japan.
[2] To whom correspondence should be addressed: Imperial College London, South Kensington, London SW7 2AZ, United Kingdom. Tel.: 44-20-7594-5327; Fax: 44-20-7594-3057; E-mail: p.freemont@imperial.ac.uk.

[3] The abbreviations used are: AAA, ATPases associated with various cellular activities; N-domain, N-terminal domain; IBMPFD, inclusion body myopathy associated with Paget disease of bone and frontotemporal dementia.

21–26), in various solution studies, including electron microscopy and small-angle x-ray scattering, the N-domain is shown to adopt more varied conformations. Positions above, coplanar with, and below the D1 ring have all been proposed. A number of models have been proposed that link the ATP hydrolysis cycle with N-domain position, but it is unknown whether the position of the N-domain drives ATPase activity of p97 or whether it moves as a result of the ATPase cycle.

p97 is directly associated with human disease, as inherited missense mutations within the p97 gene give rise to the complex disease syndrome termed inclusion body myopathy associated with Paget disease of bone and frontotemporal dementia (IBMPFD) (27). IBMPFD is a progressive autosomal dominant disorder with a myopathy that includes muscle fiber inclusions and rimmed vacuoles (28, 29). To date, 14 mutations at ten loci have been identified in p97 in IBMPFD patients (30–33). The majority of mutations are located on or near the interface between the N and D1 domains of p97 (34, 35). Although the pathogenesis of IBMPFD and the effect of mutations on the structure and function of p97 remain largely unknown, several of the IBMPFD-linked p97 mutations were reported to have higher ATPase activities and unusual N-domain conformations compared with wild-type proteins (36, 37) with crystal structures of several mutants showing small localized changes in the N-domain conformation (21).

To further elucidate the role of the N-domain in the p97 ATPase cycle, we have carried out a methodical analysis of the relationship between the N-domain and p97 ATPase activity. Firstly, we have analyzed ten major IBMPFD-associated mutants, with particular focus on the A232E mutation. We show that $p97^{A232E}$ has a significantly increased ATPase activity compared with the wild type and that this increase is due to the effect of the mutation on the N-D1 interaction. Further structure-based mutations have allowed us to probe the interaction between the N and D1 domains and investigate its effect on ATPase activity. These data lead us to propose that ATP hydrolysis by p97 critically depends on the presence of a mobile N-domain.

EXPERIMENTAL PROCEDURES

Cloning and Mutagenesis—p97 N- and C-terminal truncations were on the basis of the domain boundaries and ordered regions observed in p97 crystal structures (*e.g.* PDB code 1R7R). N-terminally truncated (residues 209–806) or C-terminally truncated (residues 9–764) murine p97 was amplified by PCR using gene-specific primers containing unique NdeI and NotI restriction endonuclease sites. The PCR products were then cloned using these sites into pET22b (Novagen) to generate constructs in frame with a C-terminal hexa-histidine tag. All mutations were introduced by PCR site-directed mutagenesis.

Expression and Purification—Protein expression in *Escherichia coli* Rosetta (DE3) cells was induced by the addition of isopropyl-β-D-thiogalactopyranoside at a final concentration of 1 mM at 22 °C. After 16 h, the cells were harvested, and the pellets were resuspended in buffer A (500 mM KCl, 2 mM β-mercaptoethanol, 25 mM HEPES (pH 8.0)) supplemented with a mixture of protease inhibitors (Sigma). After sonication and centrifugation, the supernatant was loaded onto a 5-ml HisTrap column (GE Healthcare) pre-equilibrated in buffer A. Protein was eluted with a linear imidazole gradient in buffer A. The p97-containing fractions were pooled and concentrated and further purified by gel filtration chromatography (Superose6, GE Healthcare) pre-equilibrated in buffer B (250 mM KCl, 2 mM β-mercaptoethanol, 25 mM HEPES (pH 7.5)). For cross-linking experiments, the wild type and the R155C/N387C protein were purified by the same method using the β-mercaptoethanol free buffer.

Electron Microscopy—For the negative stain grid preparation, wild-type p97 and mutant $p97^{R155C}$ and $p97^{A232E}$ samples (2 μl of 0.05 μg/ml) were applied to glow-discharged copper grids with a continuous carbon film, followed by 2% uranyl acetate solution and then blotted and air dried. For the cryo-EM sample preparation, purified p97 and p97 mutants, at a concentration of ~0.5 mg/ml, were used to prepare cryo-grids. 5 μl of sample was applied to a glow-discharged, holey carbon film on copper grids. The grids were blotted and flash frozen in liquid ethane using a Vitrobot (FEI). Data were collected under low-dose conditions on a Phillips CM200 electron microscope at the Imperial College Electron Microscopy Centre. The microscope was operating at 200 kV, using ×50,000 magnification and between 2–4 μm of nominal defocus. Images were collected using a Tietz camera.

Images were processed using IMAGIC-5 (38) except were specified. Micrographs were coarsened by a factor of 2–3.52 Å/pixel, and particles were picked interactively using BOXER in EMAN. The particles were then contrast transfer function-corrected and bandpass-filtered between 15–150 Å. Class averages were prepared from aligned particles using multivariate statistical analysis. For $p97^{A232E}$, two initial three-dimensional models were created from side views and assuming C6 symmetry. These initial models were refined using successive rounds of competitive multireference alignment (brute force alignment written by Timothy Grant) and projection matching to separate out the heterogeneity in the data and to ascertain the major conformation present. The resultant model was calculated from 1029 particles and filtered between 20–150 Å. The electron density map has been deposited in the EM data bank, accession code EMD-2038.

ATPase Assay—ATPase assays were performed at 37 °C using an NADH oxidation coupled system (39). To start the reaction, ATP (final concentration, 7 mM) was added to the preheated reaction mixture that included 1.0 μM protein, 0.35 mM NADH, 3 mM phosphoenolpyruvate, 7 units of pyruvate kinase, 23 units of lactate dehydrogenase, 100 mM Tris-HCl (pH 8.0), and 20 mM $MgCl_2$ (45). NADH oxidation was monitored by change of absorbance at 340 nm. A_{340} measurements were taken at 1-min intervals for 40 min. The ATPase activity is defined by the decrease of A_{340}/min.

Limited Proteolysis—Purified wild-type and mutant p97 proteins were diluted to 0.2 mg/ml and divided into two batches, and 4 mM of ATPγS was added to one batch. Trypsin was added to proteins to achieve a 1:100 trypsin-to-protein ratio. The mixtures were incubated at 37 °C. 10 μl of samples were extracted in 10-min intervals, mixed with 2 μl of 6× SDS sample buffer, and boiled before loading onto a 12% (v/v) SDS-PAGE gel.

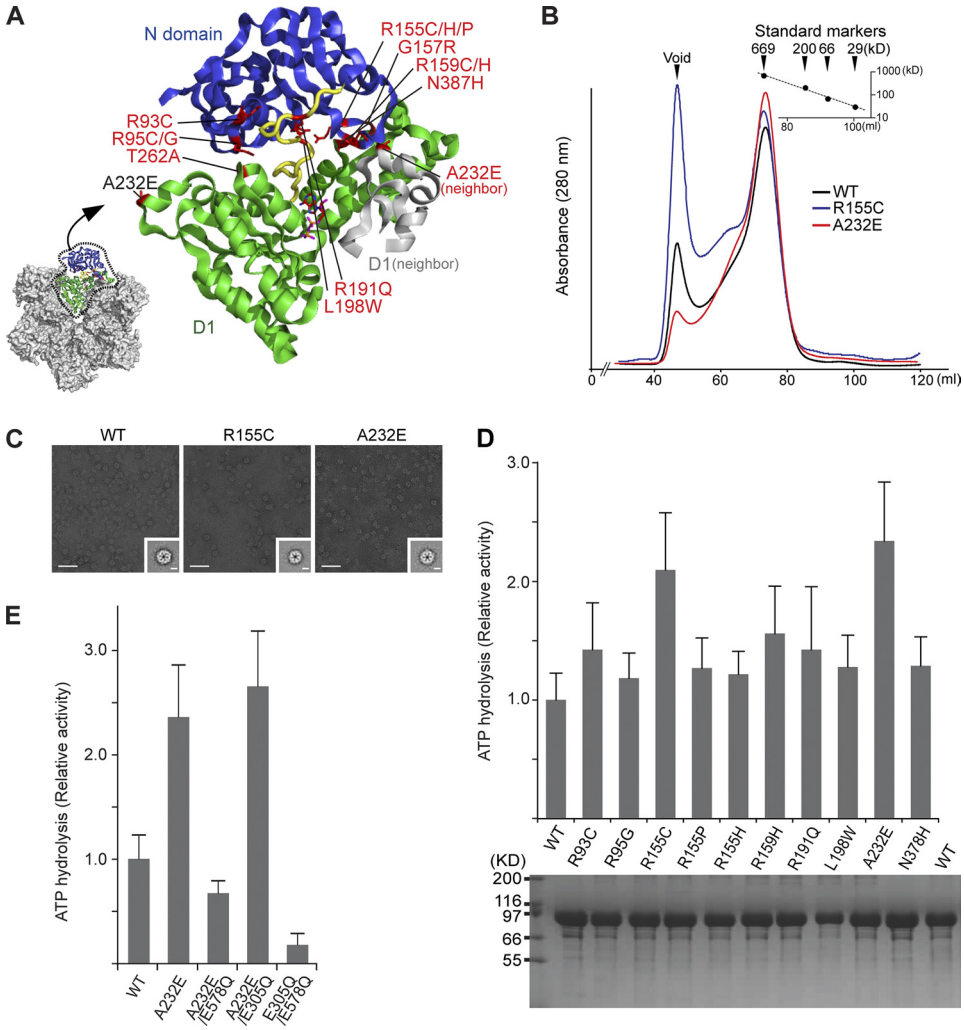

FIGURE 1. **IBMPFD-linked mutants in p97.** *A*, graphic representation of the p97 crystal structure showing the distribution of the IBMPFD-linked mutations. For clarity, only the N-domain (*blue*), the D1 domain (*green*), and the connecting linker (*yellow*) are shown. The neighboring subunits in the hexamer are shown in *gray*. *B*, typical purification profile from size-exclusion chromatography of wild-type p97 (*black*), $p97^{R155C}$ (*blue*), and $p97^{A232E}$ (*red*). The relative molecular masses (M′) of the peaks were estimated according to protein standard markers. *C*, negative-stain electron micrographs and class averages for wild-type p97, $p97^{R155C}$, and $p97^{A232E}$ with representative top-view class averages (*inset*). Class averages are the sum of 50 top-view images aligned and classified together by multivariate statistical analysis. *Scale bar* = 500 Å on the micrographs and 50 Å on the class averages. *D*, ATPase activities of wild-type p97 and ten IBMPFD mutants. The histogram shows the rates of ATP hydrolysis averaged from at least three independent measurements. *Error bars* indicate the mean ± S.D. The activities were normalized to that of wild-type. An SDS-PAGE gel of the final purified p97 proteins from size-exclusion chromatography is shown in the *lower panel*. 10 μl of each protein at 3 μM was loaded onto a 12% polyacrylamide gel followed by Coomassie Brilliant Blue staining. *E*, ATPase activities of $p97^{A232E}$ with D1 (*E305Q*) or D2 (*E578Q*) Walker B mutations. Note that only the Walker B mutation in D2 reduces the activity of $p97^{A232E}$.

RESULTS

IBMPFD Mutants Form Hexameric Ring Structures Similar to Wild-type p97—We first probed the effects of the ten major IBMPFD-linked mutations on the p97 hexamer (Fig. 1*A*). The IBMPFD-linked mutants (R93C, R95G, R155C, R155H, R155P, R159H, R191Q, L198W, A232E, and N387H) were expressed and purified, and the homogeneity and oligomeric states were assessed. A typical elution profile of p97 wild-type and IBMPFD mutants from a Superose6 gel filtration column is shown in Fig. 1*B*. All the purified mutants showed essentially the same elution profile and final purity as wild-type p97 (also see Fig. 1*D*, lower panel). The asymmetric shape of the peak suggests that multiple oligomeric species are present. We imaged samples from different fractions using negative stain electron microscopy. The void volume peak contains irreversibly aggregated material, and the shoulder fraction contains predominantly dodecameric p97 (dimer of hexamers) and some aggregates (supplemental Fig. S1), but the main component of the peak is hexameric ring-shaped p97 (Fig. 1*C*). The dodecamer and void volume fractions were found to display negligible ATPase activity showing that hexameric p97 is the only active form (supplemental Fig. S2).

IBMPFD-linked p97 Mutants Exhibit Increased ATPase Activity in D2—We next assessed the effect of IBMPFD mutations on the ATPase activity of p97. All IBMPFD mutants showed ATPase activities similar to or higher than wild-type p97 (Fig. 1*D*). The A232E and R155C mutants showed the highest increase in ATPase activities, more than double the wild-type activity (Fig. 1*D*). A Walker B double mutant (E305Q/E578Q), deficient in ATPase activity, was used throughout as a negative control. The most active IBMPFD mutant is $p97^{A232E}$, in agreement with a previous study (36, 40) and, therefore, was

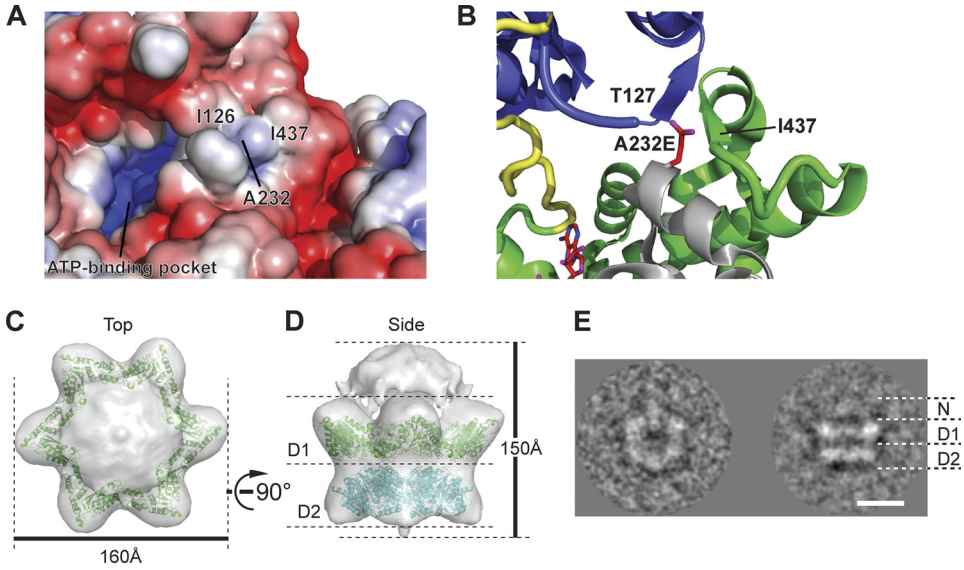

FIGURE 2. **Modeling and cryo-EM structural analysis of the p97^{A232E} IBMPFD-linked mutant.** *A*, electrostatic surface potential of p97 around A232. Hydrophobic areas are shown in *white*, with positive potential in *red* and negative potential in *blue*. *B*, a close-up view of A232 modeled with a glutamic acid side chain. Shown are top (*C*) and side (*D*) views of the cryo-EM reconstruction of p97^{A232E} at ~23 Å. Overall dimensions are indicated. The density threshold was set to account for the molecular weight of p97^{A232E}. A model of D1-D2 derived from the p97 crystal structure has been fitted into the EM envelope. The reconstruction model shows two stacked rings and a cap of density at the top. The small bottom plug is likely to be an accumulation of noise around the symmetry axis, although it may potentially be the flexible C-terminal regions. The fitted D1 and D2 domains are colored in *green* and *cyan*, respectively. *E*, cryo-EM class average of the top and side views of p97^{A232E}. *Scale bar* = 50 Å.

used for the subsequent work. To determine whether wild-type p97 and p97^{A232E} have similar secondary structures and particle sizes, circular dichroism and dynamic light scattering were performed on purified samples. The results show that both proteins have near identical secondary structures and particle size distributions (supplemental Fig. S3), suggesting that any increased ATPase activity for p97^{A232E} is not due to these factors. We also measured steady-state kinetic parameters for both wild-type p97 and p97^{A232E} (54) (supplemental Table S1). Our kinetic measurements for wild-type p97 are consistent with values published previously (19, 23, 55, 56). p97^{A232E} exhibits an increase in k_{cat}, which is consistent with the mutant having increased ATPase activity. To establish whether this increased activity p97^{A232E} is specifically due to increases in D1 or D2, we created two double mutants, combining A232E with Walker B hydrolysis mutants (E305Q in D1 or E578Q in D2). The activity of the p97$^{A232E/E305Q}$ double mutant is similar to that of p97^{A232E} (Fig. 1*E*), showing that knocking out potential ATP hydrolysis activity in D1 has no effect. In contrast, the p97$^{A232E/E578Q}$ double mutant has a significantly reduced ATPase activity (4× reduction) compared with p97^{A232E} (Fig. 1*E*). These data indicate that the increase in ATPase activity observed under steady-state conditions in p97^{A232E} is due to increased ATP hydrolysis in D2.

Cryo-EM of p97^{A232E} Indicates That the N-domains Are Flexible but Positioned above the D1 Ring—All IBMPFD mutations are clustered around the N-D1 interface of p97 (Fig. 1*A*). Therefore, we next investigated the implications of the A232E mutation on the position of the N-domain. A232 is located on the edge of the D1 domain, adjacent to the N-D1 domain interface of a neighboring subunit in the hexamer and surrounded by a hydrophobic environment including Ile-437 and Ile-126 (Fig. 2*A*). Inserting the longer glutamic acid side chain in place of alanine would disrupt the formation of a small β-sheet comprising Thr-127 in the N-domain and Ile-437 to Ala-439 in the D1 domain of the neighboring subunit (Fig. 2*B*). Thus, a potential structural consequence of A232E is to perturb the D1 domain and to disrupt the interaction between the N and D1 domains, which might result in an increased conformational flexibility of the N-domains. To explore this, cryo-EM single-particle analysis was carried out to create a three-dimensional reconstruction of the p97^{A232E} hexamer. The model shows two stacked rings corresponding to the D1 and D2 domains and a cap of density above the double rings (Fig. 2, *C* and *D*). The upper ring has a large pore, indicating that the D1 ring is open in contrast to the closed ring of existing crystal structures. The D2 ring is also slightly more open in the p97^{A232E} model than in the wild type. Model fitting of the p97 crystal structure into the EM envelope indicated a lack of corresponding density for coplanar N-domains (Fig. 2*D*), suggesting that the N-domains are in a different conformation to that observed in the crystal structures. It is plausible that the weak density on top of the D1 ring corresponds to the N-domains, but there is not enough density to account for their entire molecular weight. Conformational flexibility could account for this lack of observed density. Consistent with this, a class average from the p97^{A232E} model shows similar length D1 and D2 layers with weak extra density above D1, in the same position as in the 3D reconstruction, corresponding to the N-domains (Fig. 2*E*). Overall, the structure is very similar to our previous reconstruction of wild-type p97 in the presence of AMPPNP (44), but the N-domains of the p97^{A232E} model are even further removed from the coplanar position seen in the crystal structures. To test whether the p97^{A232E} N-D1 linker ^{A232E} is more susceptible to proteolysis, we carried out limited proteolysis on wild-type p97 and p97^{A232E} using trypsin (supplemental Fig. S4). Our results show

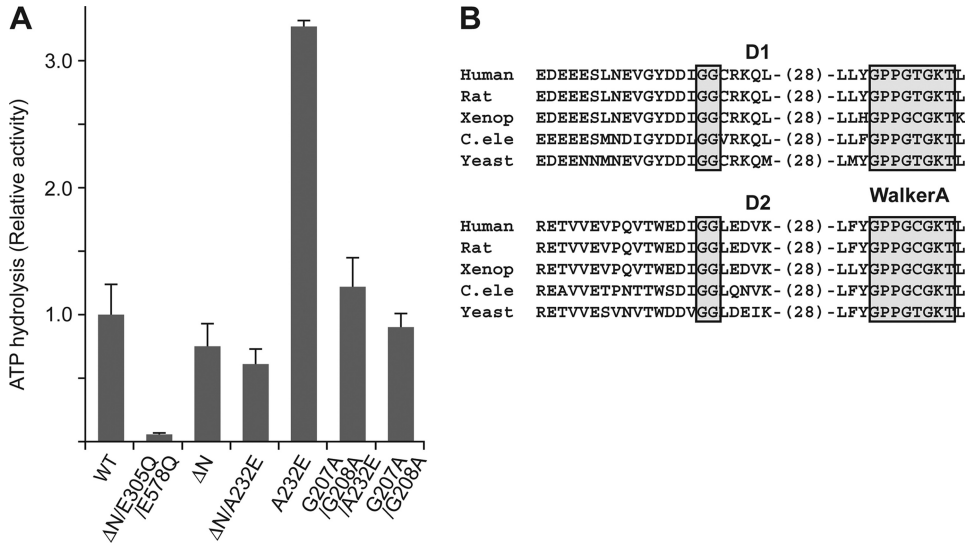

FIGURE 3. **ATPase activity of p97^{A232E} without a flexible N-domain.** *A*, ATPase activities of p97^{A232E} combined with an N-domain truncation or an N-D1 linker mutation. Measurements and presentation of results were done as for Fig. 1*D*. The D1 and D2 Walker B double-mutated p97ΔN was used as a negative control. *B*, alignment of the conserved Gly-Gly sequences in the N-D1 and D1-D2 linker regions among p97 homologs. The Gly-Gly sequences and Walker A motifs are *highlighted*.

that the N-D1 fragment from p97^{A232E} is less stable ^{A232E} than wild-type, which is consistent with a more accessible N-D1 linker for p97^{A232E}, although a destabilized D1 domain caused by possible rearrangements because of the A232E mutation cannot be ruled out.

Increased ATPase Activity of A232E Requires Flexible N-domains—We next evaluated whether the increase in ATPase activity seen for p97^{A232E} requires the presence and/or flexible nature of the N-domains. The ATPase activity of N-domain truncations of wild-type p97 (p97ΔN) and p97^{A232E} were tested. p97ΔN shows similar albeit somewhat reduced ATPase activity compared with wild-type (Ref. 25, Fig. 3*A*). Surprisingly, unlike the increased activity of A232E in full-length p97, the p97ΔN^{A232E} mutant shows similar activity to p97ΔN (Fig. 3*A*). These results suggest that N-domain plays important roles in mediating the increased ATPase activity of the A232E mutant. The significance of the increased flexible nature of p97^{A232E} was assessed next. The N-domain is connected to D1 via a linker region containing a Gly-Gly sequence that is highly conserved among p97 homologs, is similar to conserved features seen in the D1-D2 linker, (Fig. 3*B*), and could be a pivoting point for potential N-domain movement. If the increase in ATPase activity of the A232E mutation required the associated increased N-domain flexibility, mutating the Gly-Gly residues to reduce the flexibility of the N-D1 linker might negate the effect of A232E on ATPase activity. Indeed, when we mutated Gly-Gly to Ala-Ala (G207A/G208A) in p97^{A232E}, the ATPase activity was significantly reduced compared with p97^{A232E} (Fig. 3*A*), whereas the linker mutation has limited effect in the context of wild-type p97. These data suggest that the elevated ATPase activity of p97^{A232E} depends on the presence of the N-domains as well as on their increased mobility imparted by the mutation, and that wild-type p97, with its moderate ATPase activity, is less sensitive to a partially inflexible N-D1 linker.

Cross-linking between N and D1 Domains Inactivates p97 ATPase Activity—The results of the p97^{A232E} N-D1 linker mutation suggest that the increased N-domain flexibility seen in p97^{A232E} prevents proper regulation of ATP activity, suggesting that N-domain position and flexibility may play a role in modulating wild-type p97 ATP hydrolysis. To test this hypothesis, we created a mutant to reversibly lock the N-domain in a coplanar orientation, as observed in the p97 crystal structures. We did this by mutating two IBMPFD-related residues, Arg-155 and Asn-387, to cysteines. In the p97 crystal structures, these residues are close enough to form a disulfide bond (Fig. 1*A*). In non-reducing conditions, disulfide bonds would be expected to lock the N-domains in a coplanar position in the double mutant, whereas in reducing conditions the tether would be removed, allowing the N-domains to move freely. Recombinant p97$^{R155C/N387C}$ was purified in non-reducing conditions. The elution profile after size exclusion chromatography was identical to that of wild-type p97 (Fig. 4*A*), consistent with hexamer formation (*B*). Limited proteolysis and mass spectrometry confirmed a covalently linked peptide consistent with a disulfide bond between residues 155–387 (masses were determined by MS of 1545.6 Da and 1577.6 Da, corresponding to the fragment GDIFLVCGGMR/CMK). p97$^{R155C/N387C}$ was then studied by cryo-EM 2D analysis. All the class averages of p97$^{R155C/N387C}$ in non-reducing conditions show a D1 layer much wider than the D2 layer, indicating that the N-domains are locked in the D1 plane similar to what is observed in the crystal structures (Fig. 4*B*) and previous cryo-EM class averages. In ATPase assays in the absence of reducing agent, the disulfide mutant has significantly reduced activity compared with wild-type p97 (Fig. 4*C*). This effect could be reverted by the addition of the reducing agent DTT (Figs. 1*D* and 4*C*). This effect was corroborated by the k_{cat} and K_m values for the disulfide mutant with and without DTT (supplemental Table S1). It is notable that the addition of DTT to wild-type p97 also causes

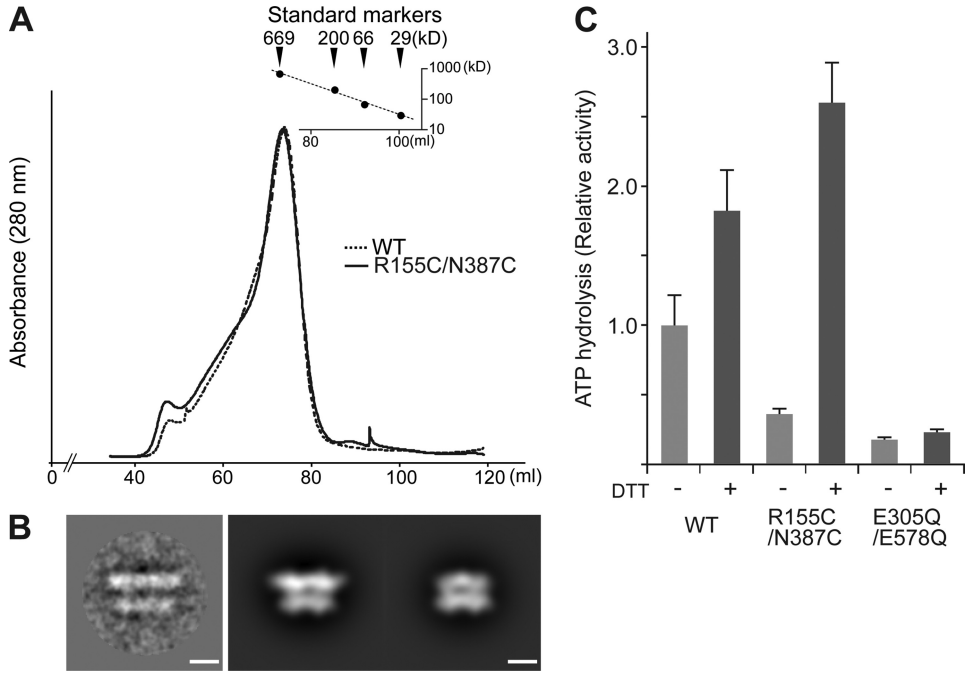

FIGURE 4. **ATPase activity of the disulfide-linked p97$^{R159C/N387C}$ mutant.** *A*, size-exclusion chromatographic profiles of wild-type p97 (*dotted line*) and the p97$^{R159C/N387C}$ cross-linked mutant (*solid line*). *B*, cryo-EM class average showing a side view of p97$^{R159C/N387C}$ in the absence of DTT (*left*) and back projections of the p97 crystal structure filtered to 25 Å resolution, with (*center*) and without (*right*) the N-domain. *Scale bars* = 50 Å. *C*, ATPase activity of p97$^{R159C/N387C}$ in the presence or absence of DTT. Measurements and representation of the histogram are the same as in Fig. 1*D*. Note that for p97$^{E305Q/E578Q}$ (D1 and D2 Walker B double mutant) there is no difference in activity with and without DTT.

a slight increase in ATPase activity. This has been observed before (41), but the reasons are unclear at present. Our data clearly show that locking the N-domain coplanar to the D1 ring correlates with an inhibition of p97 ATP hydrolysis.

The C-terminal Region of p97 Is Also Important for ATPase Activity—Even though the C-terminal region is disordered in the p97 crystal structure, biochemical data suggest important functional roles for this region (42, 43). We therefore tested whether the C-terminal region is important for p97 ATPase activity. We generated and purified C-terminally truncated wild-type p97 and A232E (p97ΔC and p97ΔC^{A232E}, respectively). Both p97ΔC and p97ΔC^{A232E} show elution profiles on size exclusion chromatography similar that to that of wild-type p97 (Fig. 5, *B* and *C*, *upper panels* and *lower left panel*). Both p97ΔC alone and in combination with the A232E mutation showed similar and significantly reduced APTase activity, approximately half that of wild-type p97 (Fig. 5*A*). Limited proteolysis reveals further similarities except in the presence of ATPγS, where p97ΔC shows decreased stability compared with wild-type p97 (Fig. 5*C*, *upper right* and *lower right panels*). This suggests that the D2 conformational change demonstrated by Wang *et al.* (20) to a tighter form induced by ATP-binding did not occur in p97ΔC. 2D cryo-EM analysis of p97ΔC revealed that there is a larger open N-D1 ring structure (162 Å in diameter) compared with wild-type p97 (149 Å), as reported previously (44) (Fig. 5*D*). These data indicate that the C-terminal region of p97 modulates the conformational changes that take place in D2 during the ATPase cycle.

DISCUSSION

IBMPFD Mutants Show Elevated ATPase Activities—In this study, we evaluated the role of N-domains in the ATPase cycle of p97 by exploring p97 mutants linked to a hereditary degenerative disorder termed IBMPFD (27). We analyzed the ATPase activities of ten major IBMPFD mutants and found that some IBMPFD mutations cause increased ATPase activities under steady-state conditions compared with wild-type p97. We then correlated increased ATPase activity with the presence of the N-domains, which was a requirement for the ATP hydrolysis-increasing effect of the A232E mutation.

Under our conditions, all the IBMPFD-linked p97 mutants have increased ATPase activities. Mutations in D1 and D2 that block ATP hydrolysis show that the elevated level of ATP turnover of p97^{A232E} is mediated by D2 and not D1. This is consistent with earlier limited-proteolysis experiments that correlated higher ATPase activity with a change in the conformation of D2 (36). Our study is the most comprehensive analysis on the ATPase activity of IBMPFD mutants and is in agreement with other studies. R95G, R155C, R155H, R155P, R191Q, and A232E have all been shown to have increased ATPase activities over wild-type p97 (34, 36, 40).

The majority of IBMPFD missense mutations cluster at the interface between the N and D1 domains (Fig. 1*A*). A number of previous studies suggest that the structural phenotype of IBMPFD is an altered N-domain conformation that is nucleotide-dependent (34, 36, 37). The general consensus is that IBMPFD mutations alter N-domain conformations, possibly promoting imbalances in cofactor binding (37). The available crystal structures of IBMPFD-linked mutants R155H and R95G (in the context of N-D1) bound to ATP directly show a relocation of the N domain relative to and above the D1 hexamer (21). However, it is possible that more drastic structural rearrangements occur as a consequence of the other IBMPFD mutations.

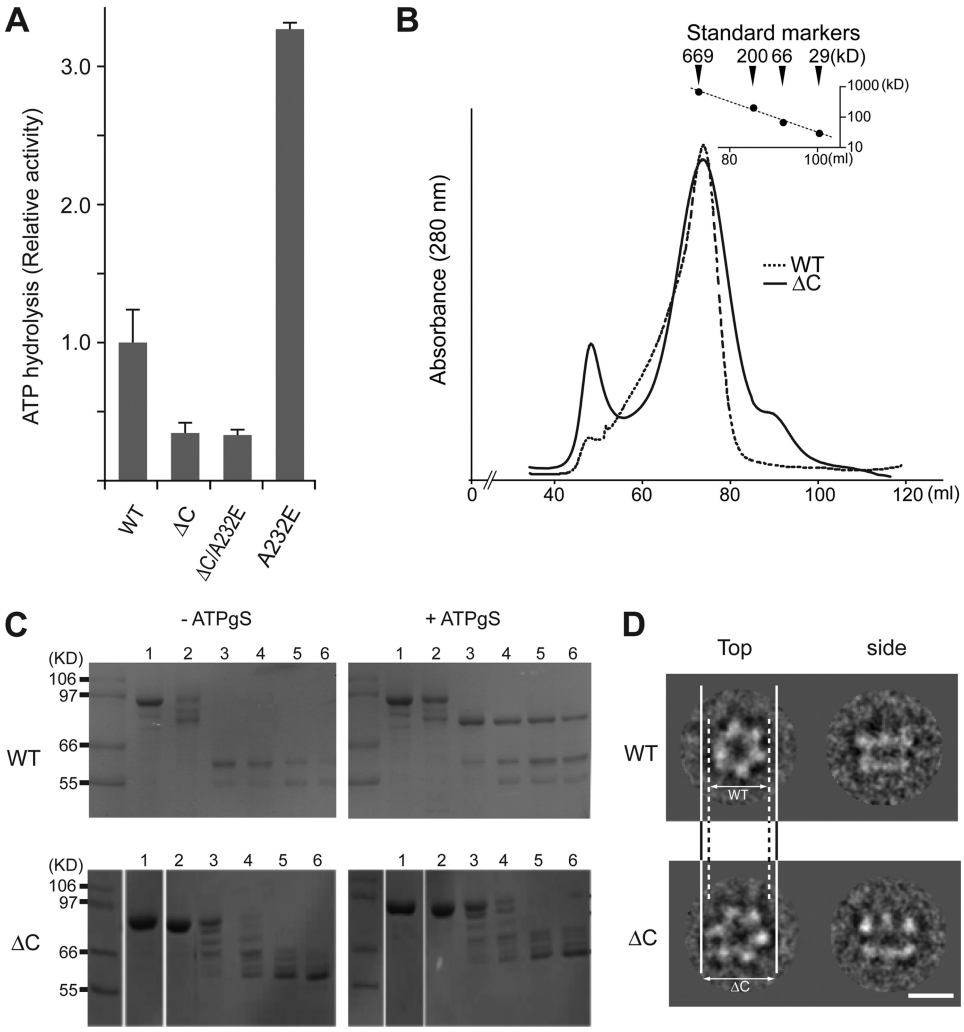

FIGURE 5. **ATPase activity of a C-terminal truncated p97.** *A*, ATPase activities of p97ΔC and p97ΔC^{A232E}. Measurements and representation of the histogram are the same as in Fig. 1*D*. *B*, typical purification profiles from size-exclusion chromatography of the wild type (*dotted line*) and ΔC (*solid line*) as shown in Fig. 1*B*. *C*, limited proteolysis for wild-type p97 and p97ΔC in the presence or absence of ATPγS. Reactions were analyzed by SDS-PAGE. Shown are *lane 1*, no trypsin; *lanes 2-6*, incubation with trypsin for 0, 10, 20, 30, and 40 min, respectively. *D*, class averages of wild-type p97 and p97ΔC cryo-EM from the top and side views with respect to the 6-fold axis. *Scale bar* = 100 Å. Note the wider opened D1 ring of p97ΔC compared with that of the wild type.

The position and chemical environment of Ala-232 as observed in p97 crystal structures suggest that the A232E mutation has a destabilizing effect on the interaction between the N and D1 domains through steric hindrance and the introduction of a negative charge in a largely hydrophobic area (Fig. 2*B*). This prediction is corroborated by both our limited proteolysis observation and by our cryo-EM reconstruction of p97^{A232E} that shows the N-domain on top of the D1 ring. The weak nature of the density also suggests that the N-domains are conformationally flexible, consistent with the N-D1 linker being more susceptible to limited proteolysis. Together, our data support the hypothesis that an increase in ATPase activity for p97^{A232E} is due to the increased flexibility of the N-domain imparted by changes in the N-D1 interface caused by the mutation. Interestingly, combining the A232E mutation with a double mutation in the N-D1 linker that is predicted to decrease its flexibility reverses the increased activity observed for p97^{A232E} alone. The removal of the N-domain in the context of the IBMPFD A232E mutant also significantly reduces ATPase activity, suggesting that the phenotype of p97^{A232E} requires a disrupted N-domain and/or linker. We cannot exclude the possibility that the linker region itself plays a role in modulating the ATPase activity of p97^{A232E}, as the same linker mutant had little effect on wild-type p97, but our structural data below strongly argues that the N-domain is more important.

The A232E mutant used in this study shows the highest increase in ATPase activity for IBMPFD mutants, which interestingly correlates with the most severe disease phenotype (28). All the IBMPFD-linked mutants tested show increased activity to some extent. However, we do not know if our biochemical findings for p97^{A232E} are the same for all the IBMPFD mutants, although it is notable that all the mutants are clustered around the N-domain and D1. It is still unclear as to how these altered biochemical properties of IBMPFD mutants affect disease pathogenesis.

N-domain Conformation and p97 ATPase Activity—Several lines of evidence support a role for N-domain conformation and flexibility in p97 ATPase activity. Firstly, the binding of p47 to p97 via the N-domain causes an inhibition of p97 ATP turnover (23). Secondly, truncation of the N-domain increases the

ATPase activity in VCP-like ATPase from Thermoplasma acidophilum (VAT), the archaeal p97 homologue (46). Thirdly, truncation of the N-domain in human p97, combined with a mutation in the D1 pore loop, increases p97 ATPase activity (47). Our data suggest that the presence of the N-domain is not required for ATPase activity but modulates it, either by constraining the flexibility of the molecule or by changes in its conformation with respect to the D1 ring being transmitted through the linker regions to the D2 ring. This is exemplified by our cross-linking data, where introducing a disulfide linkage between the N-domain and D1 abrogates p97 ATPase activity. Importantly, this is reversible by the addition of a reducing agent. All of our measurements have been carried out in the absence of adaptor proteins, and, thus, any N-domain conformational transitions may be more complex. Nevertheless, our cryo-EM data and normal mode analysis (44) support the hypothesis that N-domain and linker conformation relative to the D1-D2 hexamer ring is directly related to ATP turnover.

Effect of the C-terminal Region on p97 ATPase Activity—The C-terminal region of p97 is highly flexible, susceptible to limited proteolysis and unstructured in the p97 full-length crystal structure (15, 16). Our data suggest that the C-terminal truncation prevents D2 from undergoing the normal conformational changes upon ATP binding. For example, $p97\Delta C^{A232E}$ no longer shows the increased ATPase activity of D2 seen in $p97^{A232E}$ alone. Interestingly, this region is functionally important, as it binds adaptor proteins, including the peptide N-glycanase PNGase that is involved in endoplasmic reticulum-associated degradation substrate processing (48) and contains phosphorylation sites that modulate adaptor binding and direct subcellular localization but do not affect ATPase activity (49, 50). The C-terminal region is disordered in all p97 crystal structures solved so far, and it is difficult to propose a mechanism for how this region affects ATPase activity. It was suggested that the C-terminal region might interact directly with the N terminus of p97, a potential nuclear targeting signal, with consequences for the subcellular localization of p97 (51). Previous cryo-EM reconstructions of p97 have suggested that the C terminus may wrap around the outside of the D2 ring (52). Together with our data, this suggests that the C-terminal extension of p97 may be involved in maintaining the conformation of the D2 ring.

Model for N-domain Conformation and p97 ATPase Activity—Taken together, our results support the hypothesis that the conformation of the N-domain and linker relative to the D1-D2 hexamer is directly correlated with p97 ATPase activity. Previous models for the ATPase cycle in p97 have already suggested a role for N-domains as well as negative cooperativity between the D1 and D2 rings (15, 17, 52, 53). Our biochemical and structural data obtained from IBMPFD mutants provide experimental evidence for a model where the N-domain and linker can adopt either of two conformations, namely flexible and coplanar with D1 (Fig. 6). When the N-domains are coplanar with the D1 ring, as in the N-D1 tethered mutant and in the p97 crystal structures, ATP hydrolysis is suppressed. When the N-domains are released from the D1 plane and are in a flexible state above the double rings, D2 is competent for ATP hydrolysis. The A232E mutation (and possibly other IBMPFD mutants) hinders the ability of the N-domain to assume the coplanar conformation, leading to the observed increase in ATPase activity. In wild-type p97, N-domain conformational changes could induce transitions between an active and inactive form that are part of the p97 ATP hydrolysis cycle. Such transitions could provide the necessary force for the remodeling of target proteins via adaptor interactions.

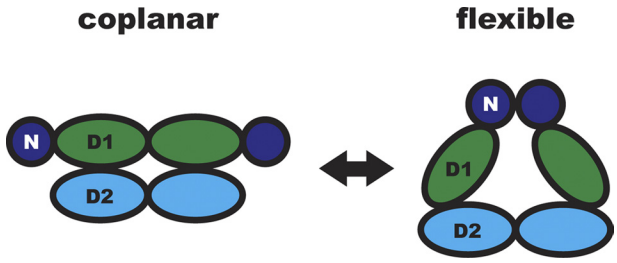

FIGURE 6. **Structural model of N-domain flexibility.** p97 can adopt two conformations in the ATPase cycle. In the "flexible" conformation, the D2 domains form a compact ring and p97 hydrolyzes ATP. When N-domains are coplanar with the D1 ring, p97 is unable to hydrolyze ATP. Only two subunits of the hexamer are shown in a side view, colored as in Figs. 1*A* and 2*D*.

Acknowledgments—We thank Andreas Förster for critical reading of the manuscript.

REFERENCES

1. Meyer, H. H., Shorter, J. G., Seemann, J., Pappin, D., and Warren, G. (2000) A complex of mammalian Ufd1 and Npl4 links the AAA-ATPase, p97, to ubiquitin and nuclear transport pathways. *EMBO J.* **19,** 2181–2192
2. Rabinovich, E., Kerem, A., Fröhlich, K. U., Diamant, N., and Bar-Nun, S. (2002) AAA-ATPase p97/Cdc48p, a cytosolic chaperone required for endoplasmic reticulum-associated protein degradation. *Mol. Cell. Biol.* **22,** 626–634
3. Bays, N. W., and Hampton, R. Y. (2002) Cdc48-Ufd1-Npl4. Stuck in the middle with Ub. *Curr. Biol.* **12,** R366–371
4. Rape, M., Hoppe, T., Gorr, I., Kalocay, M., Richly, H., and Jentsch, S. (2001) Mobilization of processed, membrane-tethered SPT23 transcription factor by CDC48(UFD1/NPL4), a ubiquitin-selective chaperone. *Cell* **107,** 667–677
5. Hetzer, M., Meyer, H. H., Walther, T. C., Bilbao-Cortes, D., Warren, G., and Mattaj, I. W. (2001) Distinct AAA-ATPase p97 complexes function in discrete steps of nuclear assembly. *Nat. Cell Biol.* **3,** 1086–1091
6. Uchiyama, K., and Kondo, H. (2005) p97/p47-Mediated biogenesis of Golgi and ER. *J. Biochem.* **137,** 115–119
7. Rabouille, C., Kondo, H., Newman, R., Hui, N., Freemont, P., and Warren, G. (1998) Syntaxin 5 is a common component of the NSF- and p97-mediated reassembly pathways of Golgi cisternae from mitotic Golgi fragments *in vitro*. *Cell* **92,** 603–610
8. Cao, K., Nakajima, R., Meyer, H. H., and Zheng, Y. (2003) The AAA-ATPase Cdc48/p97 regulates spindle disassembly at the end of mitosis. *Cell* **115,** 355–367
9. Fröhlich, K. U., Fries, H. W., Rüdiger, M., Erdmann, R., Botstein, D., and Mecke, D. (1991) Yeast cell cycle protein CDC48p shows full-length homology to the mammalian protein VCP and is a member of a protein family involved in secretion, peroxisome formation, and gene expression. *J. Cell Biol.* **114,** 443–453
10. Jarosch, E., Taxis, C., Volkwein, C., Bordallo, J., Finley, D., Wolf, D. H., and Sommer, T. (2002) Protein dislocation from the ER requires polyubiquitination and the AAA-ATPase Cdc48. *Nat. Cell Biol.* **4,** 134–139
11. Lilley, B. N., and Ploegh, H. L. (2005) Multiprotein complexes that link dislocation, ubiquitination, and extraction of misfolded proteins from the endoplasmic reticulum membrane. *Proc. Natl. Acad. Sci. U.S.A.* **102,** 14296–14301
12. Kobayashi, T., Tanaka, K., Inoue, K., and Kakizuka, A. (2002) Functional ATPase activity of p97/valosin-containing protein (VCP) is required for

the quality control of endoplasmic reticulum in neuronally differentiated mammalian PC12 cells. *J. Biol. Chem.* **277,** 47358–47365
13. Beskow, A., Grimberg, K. B., Bott, L. C., Salomons, F. A., Dantuma, N. P., and Young, P. (2009) A conserved unfoldase activity for the p97 AAA-ATPase in proteasomal degradation. *J. Mol. Biol.* **394,** 732–746
14. Ogura, T., and Wilkinson, A. J. (2001) AAA+ superfamily ATPases. Common structure, diverse function. *Genes Cells* **6,** 575–597
15. DeLaBarre, B., and Brunger, A. T. (2003) Complete structure of p97/valosin-containing protein reveals communication between nucleotide domains. *Nat. Struct. Biol.* **10,** 856–863
16. Huyton, T., Pye, V. E., Briggs, L. C., Flynn, T. C., Beuron, F., Kondo, H., Ma, J., Zhang, X., and Freemont, P. S. (2003) The crystal structure of murine p97/VCP at 3.6A. *J. Struct. Biol.* **144,** 337–348
17. Zhang, X., Shaw, A., Bates, P. A., Newman, R. H., Gowen, B., Orlova, E., Gorman, M. A., Kondo, H., Dokurno, P., Lally, J., Leonard, G., Meyer, H., van Heel, M., and Freemont, P. S. (2000) Structure of the AAA ATPase p97. *Mol. Cell* **6,** 1473–1484
18. Wang, Q., Song, C., and Li, C. C. (2003) Hexamerization of p97-VCP is promoted by ATP binding to the D1 domain and required for ATPase and biological activities. *Biochem. Biophys. Res. Commun.* **300,** 253–260
19. Song, C., Wang, Q., and Li, C. C. (2003) ATPase activity of p97-valosin-containing protein (VCP). D2 mediates the major enzyme activity, and D1 contributes to the heat-induced activity. *J. Biol. Chem.* **278,** 3648–3655
20. Wang, Q., Song, C., Yang, X., and Li, C. C. (2003) D1 ring is stable and nucleotide-independent, whereas D2 ring undergoes major conformational changes during the ATPase cycle of p97-VCP. *J. Biol. Chem.* **278,** 32784–32793
21. Tang, W. K., Li, D., Li, C. C., Esser, L., Dai, R., Guo, L., and Xia, D. (2010) A novel ATP-dependent conformation in p97 N-D1 fragment revealed by crystal structures of disease-related mutants. *EMBO J.* **29,** 2217–2229
22. Dai, R. M., Chen, E., Longo, D. L., Gorbea, C. M., and Li, C. C. (1998) Involvement of valosin-containing protein, an ATPase co-purified with IκBα and 26 S proteasome, in ubiquitin-proteasome-mediated degradation of IκBα. *J. Biol. Chem.* **273,** 3562–3573
23. Meyer, H. H., Kondo, H., and Warren, G. (1998) The p47 co-factor regulates the ATPase activity of the membrane fusion protein, p97. *FEBS Lett.* **437,** 255–257
24. Dai, R. M., and Li, C. C. (2001) Valosin-containing protein is a multi-ubiquitin chain-targeting factor required in ubiquitin-proteasome degradation. *Nat. Cell Biol.* **3,** 740–744
25. Ye, Y., Meyer, H. H., and Rapoport, T. A. (2003) Function of the p97-Ufd1-Npl4 complex in retrotranslocation from the ER to the cytosol. Dual recognition of nonubiquitinated polypeptide segments and polyubiquitin chains. *J. Cell Biol.* **162,** 71–84
26. Dreveny, I., Kondo, H., Uchiyama, K., Shaw, A., Zhang, X., and Freemont, P. (2004) Structural basis of the interaction between the AAA ATPase p97/VCP and its adaptor protein p47. *EMBO J.* **23,** 1030–1039
27. Guinto, J. B., Ritson, G. P., Taylor, J. P., and Forman, M. S. (2007) Valosin-containing protein and the pathogenesis of frontotemporal dementia associated with inclusion body myopathy. *Acta Neuropathol.* **114,** 55–61
28. Watts, G. D., Wymer, J., Kovach, M. J., Mehta, S. G., Mumm, S., Darvish, D., Pestronk, A., Whyte, M. P., and Kimonis, V. E. (2004) Inclusion body myopathy associated with Paget disease of bone and frontotemporal dementia is caused by mutant valosin-containing protein. *Nat. Genet.* **36,** 377–381
29. Haubenberger, D., Bittner, R. E., Rauch-Shorny, S., Zimprich, F., Mannhalter, C., Wagner, L., Mineva, I., Vass, K., Auff, E., and Zimprich, A. (2005) Inclusion body myopathy and Paget disease is linked to a novel mutation in the VCP gene. *Neurology* **65,** 1304–1305
30. Watts, G. D., Thomasova, D., Ramdeen, S. K., Fulchiero, E. C., Mehta, S. G., Drachman, D. A., Weihl, C. C., Jamrozik, Z., Kwiecinski, H., Kaminska, A., and Kimonis, V. E. (2007) Novel VCP mutations in inclusion body myopathy associated with Paget disease of bone and frontotemporal dementia. *Clin. Genet.* **72,** 420–426
31. Kimonis, V. E., Fulchiero, E., Vesa, J., and Watts, G. (2008) VCP disease associated with myopathy, Paget disease of bone and frontotemporal dementia. Review of a unique disorder. *Biochim. Biophys. Acta* **1782,** 744–748
32. Weihl, C. C., Pestronk, A., and Kimonis, V. E. (2009) Valosin-containing protein disease. Inclusion body myopathy with Paget's disease of the bone and fronto-temporal dementia. *Neuromuscul. Disord.* **19,** 308–315
33. Djamshidian, A., Schaefer, J., Haubenberger, D., Stogmann, E., Zimprich, F., Auff, E., and Zimprich, A. (2009) A novel mutation in the VCP gene (G157R) in a German family with inclusion-body myopathy with Paget disease of bone and frontotemporal dementia. *Muscle Nerve* **39,** 389–391
34. Weihl, C. C., Dalal, S., Pestronk, A., and Hanson, P. I. (2006) Inclusion body myopathy-associated mutations in p97/VCP impair endoplasmic reticulum-associated degradation. *Hum. Mol. Genet.* **15,** 189–199
35. Hübbers, C. U., Clemen, C. S., Kesper, K., Böddrich, A., Hofmann, A., Kämäräinen, O., Tolksdorf, K., Stumpf, M., Reichelt, J., Roth, U., Krause, S., Watts, G., Kimonis, V., Wattjes, M. P., Reimann, J., Thal, D. R., Biermann, K., Evert, B. O., Lochmüller, H., Wanker, E. E., Schoser, B. G., Noegel, A. A., and Schröder, R. (2007) Pathological consequences of VCP mutations on human striated muscle. *Brain* **130,** 381–393
36. Halawani, D., LeBlanc, A. C., Rouiller, I., Michnick, S. W., Servant, M. J., and Latterich, M. (2009) Hereditary inclusion body myopathy-linked p97/VCP mutations in the NH2 domain and the D1 ring modulate p97/VCP ATPase activity and D2 ring conformation. *Mol. Cell Biol.* **29,** 4484–4494
37. Fernández-Sáiz, V., and Buchberger, A. (2010) Imbalances in p97 co-factor interactions in human proteinopathy. *EMBO Rep.* **11,** 479–485
38. van Heel, M., Gowen, B., Matadeen, R., Orlova, E. V., Finn, R., Pape, T., Cohen, D., Stark, H., Schmidt, R., Schatz, M., and Patwardhan, A. (2000) Single-particle electron cryo-microscopy. Towards atomic resolution. *Q. Rev. Biophys.* **33,** 307–369
39. Nørby, J. G. (1988) Coupled assay of Na^+, K^+-ATPase activity. *Methods Enzymol.* **156,** 116–119
40. Manno, A., Noguchi, M., Fukushi, J., Motohashi, Y., and Kakizuka, A. (2010) Enhanced ATPase activities as a primary defect of mutant valosin-containing proteins that cause inclusion body myopathy associated with Paget disease of bone and frontotemporal dementia. *Genes Cells* **15,** 911–922
41. Noguchi, M., Takata, T., Kimura, Y., Manno, A., Murakami, K., Koike, M., Ohizumi, H., Hori, S., and Kakizuka, A. (2005) ATPase activity of p97/valosin-containing protein is regulated by oxidative modification of the evolutionally conserved cysteine 522 residue in Walker A motif. *J. Biol. Chem.* **280,** 41332–41341
42. Zhao, G., Zhou, X., Wang, L., Li, G., Schindelin, H., and Lennarz, W. (2007) Studies on peptide:N-glycanase-p97 interaction suggest that p97 phosphorylation modulates endoplasmic reticulum-associated degradation. *Proc. Natl. Acad. Sci. U.S.A.* **104,** 8785–8790
43. Böhm, S., Lamberti, G., Fernández-Sáiz, V., Stapf, C., and Buchberger, A. (2011) Cellular functions of Ufd2 and Ufd3 in proteasomal protein degradation depend on Cdc48 binding. *Mol. Cell. Biol.* **31,** 1528–1539
44. Beuron, F., Dreveny, I., Yuan, X., Pye, V. E., McKeown, C., Briggs, L. C., Cliff, M. J., Kaneko, Y., Wallis, R., Isaacson, R. L., Ladbury, J. E., Matthews, S. J., Kondo, H., Zhang, X., and Freemont, P. (2006) Conformational changes in the AAA ATPase p97-p47 adaptor complex. *EMBO J.* **25,** 1967–1976
45. Tanner, J. A., Abowath, A., and Miller, A. D. (2002) Isothermal titration calorimetry reveals a zinc ion as an atomic switch in the diadenosine polyphosphates. *J. Biol. Chem.* **277,** 3073–3078
46. Gerega, A., Rockel, B., Peters, J., Tamura, T., Baumeister, W., and Zwickl, P. (2005) VAT, the thermoplasma homolog of mammalian p97/VCP, is an N domain-regulated protein unfoldase. *J. Biol. Chem.* **280,** 42856–42862
47. Rothballer, A., Tzvetkov, N., and Zwickl, P. (2007) Mutations in p97/VCP induce unfolding activity. *FEBS Lett.* **581,** 1197–1201
48. Yeung, H. O., Kloppsteck, P., Niwa, H., Isaacson, R. L., Matthews, S., Zhang, X., and Freemont, P. S. (2008) Insights into adaptor binding to the AAA protein p97. *Biochem. Soc. Trans.* **36,** 62–67
49. Ewens, C. A., Kloppsteck, P., Förster, A., Zhang, X., and Freemont, P. S. (2010) Structural and functional implications of phosphorylation and acetylation in the regulation of the AAA+ protein p97. *Biochem. Cell Biol.* **88,** 41–48
50. Egerton, M., and Samelson, L. E. (1994) Biochemical characterization of valosin-containing protein, a protein tyrosine kinase substrate in hemato-

poietic cells. *J. Biol. Chem.* **269,** 11435–11441
51. Madeo, F., Schlauer, J., Zischka, H., Mecke, D., and Fröhlich, K. (1998) Tyrosine phosphorylation regulates cell cycle-dependent nuclear localization of Cdc48p. *Mol. Biol. Cell* **9,** 131–141
52. Rouiller, I., DeLaBarre, B., May, A. P., Weis, W. I., Brunger, A. T., Milligan, R. A., and Wilson-Kubalek, E. M. (2002) Conformational changes of the multifunction p97 AAA ATPase during its ATPase cycle. *Nat. Struct. Biol.* **9,** 950–957
53. Pye, V., Dreveny, I., Briggs, L., Sands, C., Beuron, F., Zhang, X., and Freemont, P. (2006) Going through the motions: the ATPase cycle of p97. *J. Struct. Biol.* **156,** 12–28
54. Cogan, E. B., Birrell, G. B., and Griffith, O. H. (1999) A robotics-based automated assay for inorganic and organic phosphates. *Anal. Biochem.* **271,** 29–35
55. DeLaBarre, B., Christianson, J. C., Kopito, R. R., and Brunger, A. T. (2006) Central pore residues mediate the p97/VCP activity required for ERAD. *Mol. Cell* **22,** 451–462
56. Zalk, R., and Shoshan-Barmatz, V. (2003) ATP-binding sites in brain p97/VCP (valosin-containing protein), a multifunctional AAA ATPase. *Biochem. J.* **374,** 473–480